Available online at www.sciencedirect.com

ScienceDirect

www.elsevier.com/locate/jes

JES JOURNAL OF ENVIRONMENTAL SCIENCES www.jesc.ac.cn

Bioaccumulation characterization of uranium by a novel *Streptomyces sporoverrucosus* dwc-3

Xiaolong Li[1], *Congcong Ding*[1,2], *Jiali Liao*[1,*], *Liang Du*[3], *Qun Sun*[2], *Jijun Yang*[1], *Yuanyou Yang*[1], *Dong Zhang*[3], *Jun Tang*[1], *Ning Liu*[1,*]

1. *Key Laboratory of Radiation Physics and Technology, Ministry of Education, Institute of Nuclear Science and Technology, Sichuan University, Chengdu 610064, China. E–mail: lixiaolongscu720@126.com*
2. *Key Laboratory of Biological Resource and Ecological Environment of the Ministry of Education, College of Life Sciences, Sichuan University, Chengdu 610064, China*
3. *Institute of Nuclear Physics and Chemistry, CAEP, Mianyang 621900, China*

ARTICLE INFO

Article history:
Received 16 January 2015
Revised 1 April 2015
Accepted 23 June 2015
Available online 12 August 2015

Keywords:
Bioaccumulation
Uranium
Nanoparticle
Streptomyces sporoverrucosus dwc-3
Bioremediation

ABSTRACT

The biosorption mechanisms of uranium on an aerobic bacterial strain *Streptomyces sporoverrucosus* dwc-3, isolated from a potential disposal site for (ultra-)low uraniferous radioactive waste in Southwest China, were evaluated by using transmission electron microscopy (TEM), energy dispersive X-ray (EDX) analysis, Fourier transform infrared spectroscopy (FT-IR), X-ray photoelectron spectroscopy (XPS), proton induced X-ray emission (PIXE) and enhanced proton backscattering spectrometry (EPBS). Approximately 60% of total uranium at an initial concentration of 10 mg/L uranium nitrate solution could be absorbed on 100 mg *S. sporoverrucosus* dwc-3 with an adsorption capacity of more than 3.0 mg/g (wet weight) after 12 hr at room temperature at pH 3.0. The dynamic biosorption process of *S. sporoverrucosus* dwc-3 for uranyl ions was well described by a pseudo second-order model. *S. sporoverrucosus* dwc-3 could accumulate uranium on cell walls and within the cell, as revealed by SEM and TEM analysis as well as EDX spectra. XPS and FT-IR analysis further suggested that the absorbed uranium was bound to amino, phosphate and carboxyl groups of the cells. Additionally, PIXE and EPBS results confirmed that ion exchange also contributed to the adsorption process of uranium.

Introduction

Environmental contamination by uranium has increased due to anthropogenic activities, such as mining, manufacture of nuclear weapons, nuclear energy production and storage of radioactive wastes (Gadd and Fomina, 2011; Li et al., 2014; Pang et al., 2011). Release of uranium is of major public concern because of its severe threat to the health of human beings and to the diversity, structure and function of affected ecosystems (Gorman-Lewis et al., 2005; Williams et al., 2013). Moreover, its biologically dynamic toxicity, metabolic toxicity and chemical toxicity could lead to potential long-term harm to mammalian reproduction and reduce biological fertility, and lead to abnormal and slow embryonic development (Bai et al., 2010; Donat, 2009; Schmeide et al., 2003; Xie et al., 2009; Vogel et al., 2010; Wang et al., 2010). The World Health Organization has determined that uranium is a human carcinogen and its concentration in water should not exceed 50 μg/L (Han et al., 2007; Shin et al., 2002). Therefore, the fate and mobility of uranium should be given more attention

* *Corresponding authors*. E-mails: liaojiali@scu.edu.cn (Jiali Liao), nliu720@scu.edu.cn (Ning Liu).

http://dx.doi.org/10.1016/j.jes.2015.06.007
1001-0742/

when uraniferous radioactive wastes find their way into the environment.

Precipitation, filtration, coagulation, evaporation, ion exchange, membrane separation and solvent extraction are conventional physicochemical methods used for uranium remediation. However, application of these methods is always expensive, not environmentally friendly and usually dependent on the concentration of the waste (Zhang et al., 2014). More specifically, the traditional methods are sometimes restricted at low metal concentrations of 1–100 mg/L (Lin et al., 2012; Mao et al., 2011; Pagnanelli et al., 2000; Vijayaraghavan and Yun, 2008). Therefore, there is a great need for an alternative technique that is both economical and efficient. Of possible options, biosorption is becoming one of the most attractive alternative methods and has distinct advantages over conventional methods (Li et al., 2010; Wang and Chen, 2009; Wang et al., 2010). Compared with traditional methods, the major advantages of biosorption include low cost, high efficiency, minimization of chemical and biological sludge and regeneration of the biosorbent. Moreover, given these promising results, biosorption is now being considered for the recycling of waste materials.

Over the last two decades, many researchers have reported the removal of uranium using various microorganisms, such as bacteria (Li et al., 2011; Mohamed and Sonja, 2008; Selenska-Pobell et al., 2001; Suzuki and Banfield, 2004), actinomycetes (Golab et al., 1991; Schmidt et al., 2009), fungi (Ding et al., 2014b; Gadd and Fomina, 2011) and yeasts (Lu et al., 2013; Ohnuki et al., 2005; Wang and Chen, 2006). However, heavy metal adsorption appears to be stronger using Gram-positive cell walls than using Gram-negative cell walls. Gram-positive bacteria such as *Streptomyces* have a large heavy metal binding capacity resulting from numerous functional groups, such as carboxyl and phosphoryl groups, on the cell wall (carboxyl groups present on peptidoglycan and phosphoryl groups primarily on teichoic acid of Gram-positive bacteria cell walls) (Rho and Kim, 2002). Besides, some *Streptomyces* species exhibit tolerance to different metals and have relatively high biosorption capacities (Chergui et al., 2007; Schmidt et al., 2009; Yuan et al., 2009). In the recent literature, more and more *Streptomyces* strains have been employed as biosorbents in the removal of metal ions such as Cu^{2+}, Zn^{2+}, Cr^{6+}, Pb^{2+}, Cd^{2+} and UO_2^{2+} (Chergui et al., 2007; Friis and Myers, 1986; Golab et al., 1991). However, knowledge on the bioaccumulation characteristics of metals, especially uranium, by *Streptomyces*, as well as their intracellular and extracellular distribution, is still limited.

In the present study, *Streptomyces sporoverrucosus* dwc-3, one of the dominant actinomycic species, was isolated from a potential disposal site of (ultra-)low uraniferous radioactive waste in Southwest China. Then, the biosorption characteristics of uranium by living cells of *S. sporoverrucosus* dwc-3 were investigated using transmission electron microscopy (TEM), energy dispersive X-ray (EDX) analysis, Fourier transform infrared spectroscopy (FT-IR), X-ray photoelectron spectroscopy (XPS), proton induced X-ray emission (PIXE) and enhanced proton backscattering spectrometry (EPBS). These results could contribute to a better understanding of biosorption mechanisms and be helpful in the development of potential biosorbents for uranium uptake from aqueous environments.

1. Materials and methods

1.1. Chemical reagents

Unless stated otherwise, all the chemical reagents used were analytical grade. Uranium stock solution of 1 g/L was prepared by dissolving uranyl nitrate hexahydrate ($UO_2(NO_3)_2{\cdot}6H_2O$) (Aladdin Chemistry Co., Ltd., Shanghai, China) in distilled water. The stock solution was kept in an acidic condition, and working solutions with U(VI) concentration equaling to 1–100 mg/L were prepared by appropriate dilution of the stock solution immediately before experiments.

1.2. Strain isolation and cultivation

The actinomycic strain used in the present work was isolated from the aerated zone soil, collected from a potential site for radioactive waste disposal at a depth of 3.5 m below the land surface, located in Sichuan province (China). The microbial communities of the soil samples were analyzed using the spread plate method with three kinds of general medium (bacteria, fungi, and actinomycete). Then the colony with the largest number on actinomycetic agar was selected and purified. The isolate was identified as *S. sporoverrucosus* dwc-3 *via* 16S rRNA. The actinomycete was incubated in Gause's medium (Ding et al., 2014a) (medium composition: 20 g solute starch; 0.5 g NaCl; 1 g KNO_3; 0.5 g $K_2HPO_3{\cdot}3H_2O$; 0.5 g $MgSO_4{\cdot}7H_2O$; 0.01 g $FeSO_4{\cdot}7H_2O$; 1000 mL H_2O; pH 7.4–7.6). All the chemical reagents used in this medium were purchased from Chengdu Kelong Chemical Reagent Co., Ltd. (Chengdu Kelong Chemical Reagent Co., Ltd., Chengdu, China). *Streptomyces* cells used for experiment were harvested from a 6 day culture suspension at 30°C by centrifugation (4000 r/min) for 5 min and washed three times in distilled water.

1.3. Biosorption experiments

All the biosorption experiments were carried out under ambient conditions, except as otherwise described. The batch experimental method was performed in triplicate and the process was as follows: the desired pH values of uranium stock solution were first adjusted using dilute HNO_3 and NaOH solution. Then 100 mg of *S. sporoverrucosus* dwc-3 cells (wet weight) was added and allowed to contact with 20 mL of the uranium solution at a fixed temperature until the reaction reached equilibrium. After 12 hr, the suspension was centrifuged (5000 r/min, 20 min) and the uranium concentration was analyzed by ultraviolet–visible (UV–Vis) spectrophotometer (UV-2450, SHIMADZU Corporation, Japan) with arsenazo (III) as the complexing agent.

The sorption ratio R (%) and adsorption capacity Q (mg/g) were calculated from the following equations:

$$R = \frac{C_0 - C}{C_0} \times 100\% \quad (1)$$

$$Q = \frac{(C_0 - C) \times V}{W} \quad (2)$$

where C_0 and C (mg/L) are the concentrations of the uranium in the initial and final solutions, respectively, V (L) is the

volume of the solution and W (g) is the weight of the bacterial cells.

1.4. FT-IR analysis

FTIR spectroscopic analysis was performed to determine the potential functional groups and possible binding sites involved in uranium biosorption. For the U-loaded sample, the *S. sporoverrucosus* dwc-3 cells were exposed in U(VI) solution with a concentration of U(VI) of 10 mg/L and pH 3.0. After 12 hr, the suspension was centrifuged (5000 r/min, 20 min), the supernatant was removed and the U-loaded cells were washed in distilled water to remove the remaining uranium solution. Finally, the control cells and U-loaded *S. sporoverrucosus* dwc-3 cells were lyophilized and blended with KBr. The infrared spectra were recorded within the range 400–4000 cm^{-1} using a FTIR spectrometer (Nicolet 6700, Thermo Electron Corporation, USA).

1.5. XPS analysis

The XPS spectroscopy technique was used to identify the interaction mechanism between uranium and *S. sporoverrucosus* dwc-3. The original cells and the uranium-loaded *S. sporoverrucosus* dwc-3 cells were lyophilized before XPS analysis using the Al Kα line in an Axis-Ultra instrument (XSAM800, Kratos, UK). The XPS analysis chamber was operated at 10^{-9} Torr, the experimental resolution was estimated to be 0.5 eV, and the analyzer was set at 20 eV pass energy.

1.6. SEM-EDS and TEM-EDX analyses

SEM-EDS (energy dispersive spectrometer) and TEM-EDX analyses were applied to establish the cellular localization of the adsorbed uranyl ions and the elemental characterization of the metal precipitates.

Samples of original cells (control) and uranium-loaded cells were prepared for electron microscopy analyses by fixation for 4 hr at 4°C in 2.5% glutaraldehyde in sodium phosphate buffer (0.1 mol/L, pH 7.2) and then washed three times with the same sodium phosphate buffer. For SEM-EDS analysis (S4800, Hitachi, Japan), the dehydrated samples were dried using the critical point drying method, sputter-coated with gold, and then mounted on stubs for viewing in the SEM. For TEM-EDX analysis (Tecnai G2 F20 S-TWIN, FEI, USA), the cell pellets were fixed for 60 min at 4°C in OsO_4 in phosphate buffer before being dehydrated through a graded ethanol series. The dehydrated samples were embedded in epoxy resins and sectioned into ultra-thin specimens. Thin sections were supported on copper grids for morphological study after staining with lead citrate.

1.7. EPBS and PIXE analyses

For EPBS and PIXE analyses, the original cells and the uranium (U)-loaded *S. sporoverrucosus* dwc-3 cells were lyophilized and pressed to form a pellet. EPBS and PIXE were carried out on a Van de Graaff accelerator (J-2.5, Xianfeng Electrical Machinery Factory, China) in the Institute of the Nuclear Science and Technology at Sichuan University, China. The EPBS spectra were recorded at a scattering angle of 165° by an Au (Si) detector with depletion depth of 100 μm. The PIXE spectra were detected at an angle of 135° by a Si (Li) detector. The EPBS and PIXE spectra were analyzed using computer code SIMNRA (Max-Planck-Institut für Plasmaphysik, Garching, Germany) and GUPIXWIN (University of Guelph, Guelph, Ontario, Canada), respectively.

2. Results and discussion

2.1. Kinetic studies

The effect of contact time on uranium biosorption by *S. sporoverrucosus* dwc-3 is shown in Fig. 1. It is clear that the biosorption of uranium occurred rapidly over a period of 0–5 hr, then reached equilibrium after 12 hr. The maximum value of sorption rate was about 60%. In the subsequent experiments, a 12 hr reaction time was selected to ensure the achievement of biosorption equilibrium.

In order to describe the dynamic biosorption process of U(VI) by *S. sporoverrucosus* dwc-3, the kinetic data were described using pseudo-first-order and pseudo-second-order rate equations. The linear forms of the pseudo-first-order model and pseudo-second-order are given in Eqs. (3) and (4) (Largergren, 1898; Ho, 2006), respectively:

$$\ln(q_e - q_t) = \ln q_e - k_f \times t \tag{3}$$

$$\frac{t}{q_t} = \frac{1}{k_s q_e^2} + \frac{t}{q_e} \tag{4}$$

where q_e and q_t (mg/g) are the concentration of U(VI) adsorbed on the biosorbent at equilibrium and at time t, respectively, k_f (min^{-1}) and k_s (mg/(g·min)) are the pseudo-first-order and pseudo-second-order kinetic rate constants, respectively. As

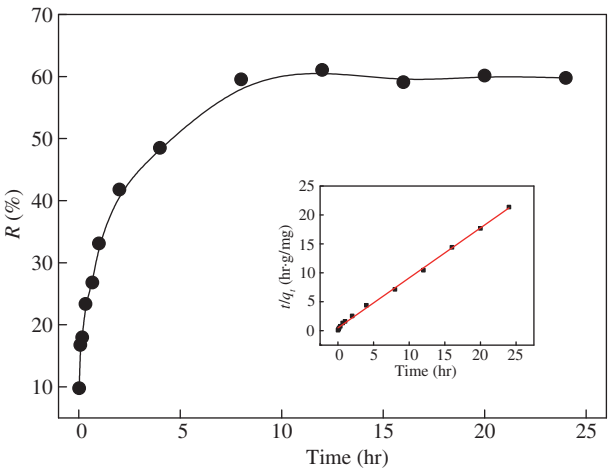

Fig. 1 – Biosorption kinetics of U(VI) on *S. sporoverrucosus* dwc-3. Adsorption conditions: initial concentration of U(VI) (C_0) = 10.0 mg/L, pH = 3.0, the concentration of *S. sporoverrucosus* dwc-3 cells (*M/V*) = 5.0 g/L, and sorption temperature (*T*) = 30°C. Inset curve shows the fitting of the pseudo-second-order kinetic model. *R*: sorption ratio; t: sorption time; q_t: concentration of U(VI) adsorbed at time t.

shown in Fig. 1, the adsorption of U(VI) on *S. sporoverrucosus* dwc-3 is better simulated by a pseudo-second-order kinetic model ($R^2 > 0.99$) compared to the pseudo-first-order model (data not shown). The biosorption kinetics indicates that the chemisorption of U(VI) on *S. sporoverrucosus* dwc-3 is the rate-limiting step. Lin et al. (2012) also found that the biosorption of divalent metal ions like Zn^{2+} and Cd^{2+} on *Streptomyces zinciresistens* CCNWNQ 0016^T could be well fitted by a pseudo-second order kinetic model ($R^2 > 0.99$).

2.2. Effect of pH

The effect of pH on U(VI) biosorption on *S. sporoverrucosus* dwc-3 was investigated by the batch technique (Fig. 2). In order to avoid uranyl ion complexation caused by high pH, the pH range from 1.0 to 7.0 was chosen in the pH experiments. As illustrated in Fig. 2a, U(VI) biosorption increased from pH 1.0 to 4.0, and then maintained this level at pH 4.0–7.0, with nearly 100% of U(VI) adsorbed by 100 mg of *S. sporoverrucosus* dwc-3. The pH value was the most significant environmental factor affecting the U(VI) biosorption. It can not only influence protonation or deprotonation of functional groups on the cell surface, but also determine the U(VI) speciation in aqueous solution (Lu et al., 2013; Vogel et al., 2010). The electrostatic interaction between the *S. sporoverrucosus* dwc-3 surface and uranyl ions, therefore, was remarkably influenced.

Additionally, the speciation of U(VI) depends on the concentration of uranium, pH values, ionic strength, and addition of CO_2. According to the distribution of uranium species shown in Fig. 2b, computed by Visual MINTEQ 3.0, soluble uranium species like UO_2^{2+} predominate in the solution below pH 4.0. As the pH of the solution increased (pH > 4.0), hydrolysis of uranium increased and formed various hydroxy complexes of U(VI). At pH ~7.0, the dominant species are $(UO_2)_2(OH)_5^+$ (~73.4%), $UO_2(OH)_2$(aq) (~12.4%), UO_2OH^+ (~9.9%), and $(UO_2)_4(OH)_7^+$ (~2.8%). Above pH 9.0–10.0, $UO_2(OH)_3^-$ dominates, and other species are negligible. Thus, the biosorption experiments for uranium in this study were carried out at a low pH value (pH 3.0), where the uranium solution speciation is dominated by highly mobile uranyl ions.

2.3. Biosorption isotherms

Biosorption isotherms of U(VI) on *S. sporoverrucosus* dwc-3 are displayed in Fig. 3. As shown in the figure, the biosorption of U(VI) on *S. sporoverrucosus* dwc-3 increased with the increasing solution concentration. Meanwhile, Fig. 3 also shows that the sorption ratio was affected by temperature over a range of 10–40°C, which revealed that uranium biosorption by *S. sporoverrucosus* dwc-3 was dependent on temperature. Over the temperature range tested (10–40°C), the biosorption capacity of uranium increased from 2.4 to 3.9 mg/g (wet weight) at initial U(VI) concentration of 100 mg/L. The increase of biosorption capacity might result from enhancement of the surface activity of the cells and kinetic energy of the solution by the higher temperature. Finally, a temperature of 30°C was selected for the subsequent batch experiments.

Furthermore, the Langmuir and Freundlich models were applied in the equilibrium analysis to understand the biosorption mechanisms. The Langmuir model assumes monolayer type adsorption and supposes that all the active sites on the sorbent surface have the same affinity with the adsorbate, while the Freundlich isotherm model, an empirical expression, depicts heterogeneous adsorption with exponential distribution of the sites and their energies (Stumm, 1992). The linear forms of the Langmuir and Freundlich equations can be expressed as Eqs. (5) and (6) (Langmuir, 1918; Freundlich, 1906), respectively:

$$\frac{C_e}{q_e} = \frac{C_e}{q_{max}} + \frac{1}{q_{max}K_L} \tag{5}$$

$$\log q_e = \log K_F - (1/n)\log C_e \tag{6}$$

where q_e (mg/g) is the adsorbed amount at equilibrium, C_e (mg/L) is the equilibrium concentration of the adsorbate in solution, q_{max} (mg/g) is the Langmuir monolayer sorption capacity, K_L (L/mg) is the Langmuir equilibrium constant, $1/n$ is the heterogeneity of the adsorption sites, and K_F represents the equilibrium coefficient, which describes the partitioning of the adsorbate between the solid and liquid phases over the concentration range studied.

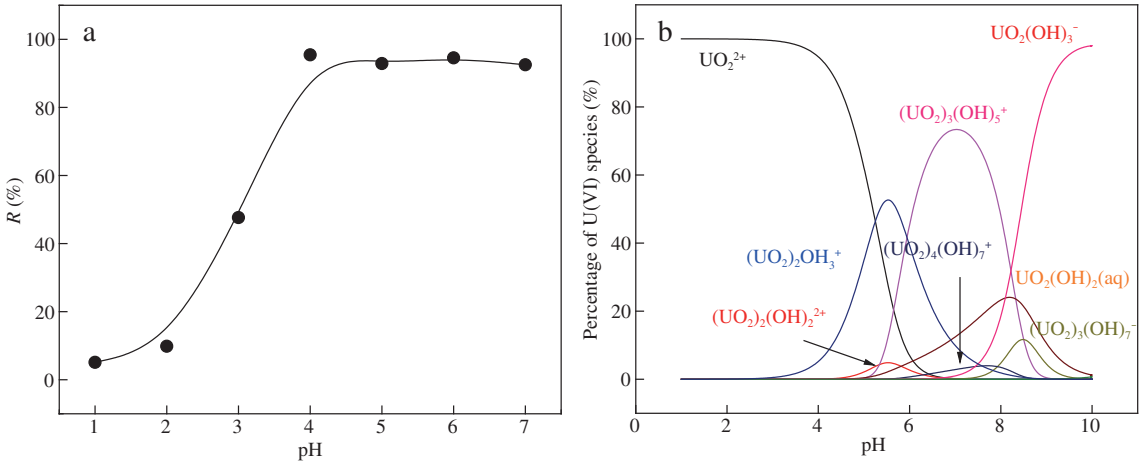

Fig. 2 – Effect of pH on (a) U(VI) biosorption by *S. sporoverrucosus* dwc-3 and (b) speciation of U(VI) in solution. Adsorption conditions: C_0 = 10.0 mg/L, M/V = 5.0 g/L, and T = 30°C. Calculation made with Visual MINTEQ 3.0.

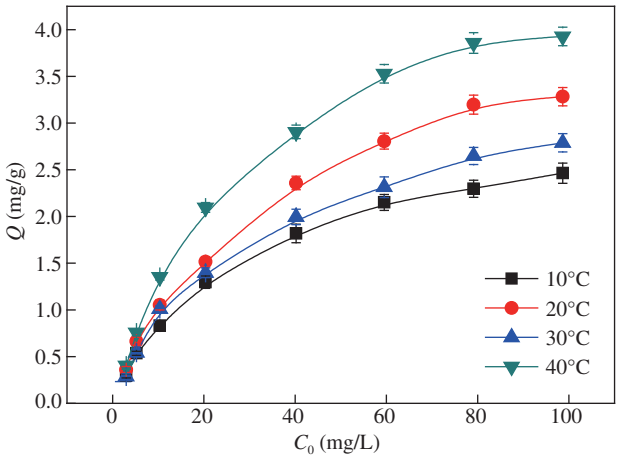

Fig. 3 – Biosorption isotherms of U(VI) by *S. sporoverrucosus* dwc-3 at different temperatures. Adsorption conditions: pH = 3.0 and M/V = 5.0 g/L. Q: adsorption capacity.

The biosorption isotherms of U(VI) by *S. sporoverrucosus* dwc-3 at 30°C were fitted by Langmuir and Freundlich models, and their relative parameters calculated from the two models are listed in Table 1. As tabulated in Table 1, one can see that the biosorption of U(V) by *S. sporoverrucosus* dwc-3 can be better fitted by the Freundlich model (R^2 = 0.996) than the Langmuir model (R^2 = 0.934) at 30°C, suggesting that the biosorption of U(VI) by *S. sporoverrucosus* dwc-3 may follow a heterogeneous model, and other mechanisms such as intracellular bioaccumulation would contribute to the uptake of UO_2^{2+} in addition to surface binding (Kaduková and Virčíková, 2005; Li et al., 2010). The maximum U(VI) biosorption capacity of *S. sporoverrucosus* dwc-3 calculated from the Langmuir model at pH 3.0 and T = 30°C was 2.07 mg/g. In addition, in the case of Freundlich isotherm model, the *n* value is 2.44, between 1 and 10, indicating that the biosorption for U(VI) was favorable under the studied conditions.

2.4. FT-IR spectroscopy

FT-IR spectra were examined for control (metal-free) and uranium-loaded cells between 4000 and 400 cm^{-1} in order to elucidate the functional groups involved in uranium binding. Assignments of characteristic peaks in the present study were based on known data from the literature (Choudhary and Sar, 2011; Kazy et al., 2009; Kushwaha et al., 2012; Ojeda et al., 2008).

Table 1 – Parameters of models for U(VI) biosorption on *Streptomyces sporoverrucosus* dwc-3.

Metal	Langmuir model			Freundlich model		
	K_L (mg^{-1})	q_{max} (mg/g)	R^2	1/*n*	K_F (g^{-1})	R^2
U(VI)	1.81	2.07	0.934	0.41	0.57	0.996

K_L: the Langmuir equilibrium constant; q_{max}: the Langmuir monolayer sorption capacity; 1/*n*: the heterogeneity of the adsorption sites; K_F: the equilibrium coefficient.

The FT-IR spectra of control cells and uranium loaded cells are shown in Fig. 4. It can be seen that a broad band between 3500 and 3200 cm^{-1} with a maximum around 3300 cm^{-1}, which was due to the stretching of the N–H bond of amino groups and also due to the presence of out-plane flexural vibration of the hydroxyl groups (γO–H), usually appeared in the region between 3800 and 3200 cm^{-1}.

Two FT-IR spectra showed the presence of two peaks between 3000 and 2900 cm^{-1}, which could be assigned to the asymmetric stretching of C–H bond of the $–CH_2$ groups combined with that of the $–CH_3$ groups, indicating the presence of protein-related bonds.

The broad band between 1700 and 1470 cm^{-1} could be attributed to amide groups. The typical amide I band, from the C═O stretching vibration of amide, appeared strongly at 1655.4 cm^{-1}. The peak at 1540.6 cm^{-1}, known as amide II, was contributed by a motion combining both the –NH bending and the –CN stretching vibration. The spectrum of uranium-loaded cells showed minor shifts of these two bands to 1658.4 and 1538.3 cm^{-1}, respectively.

The small absorbance peak at 1456.1 cm^{-1} was characteristic of the $–CH_2$ scissoring motion or $–CH_3$ antisymmetrical bending vibration. A minor shift of the peak at 1378.3 to 1384.1 cm^{-1} due to the symmetric stretching vibration of COO^- indicated the role of carboxyl groups in metal binding. In the control spectrum, absorption peaks at 1237.7 and 1080.3 cm^{-1} were observed due to vibrations of carboxyl (–COOH) and phosphate groups (P═O and P–O of the $C–PO_3^{2-}$ moiety), and a shift of these peaks to 1235.0 and 1079.7 cm^{-1} after cell exposure to uranium suggested the interaction of bound metals with carboxyl and phosphate groups. Changes in peak position and intensity in the 800 to 400 cm^{-1} region could be assigned to the in-plane flexural vibration of intense M–O (δ(M–O)) and O–M–O (δ(O–M–O)) bonds (M = metal ion). In the uranium-loaded sample, the appearance of a new peak at 922.6 cm^{-1} and changes in peak positions and intensity around 550–1000 cm^{-1} region could be assigned to asymmetric stretching vibration of $\nu_3(UO_2^{2+})$ and stretching vibrations of

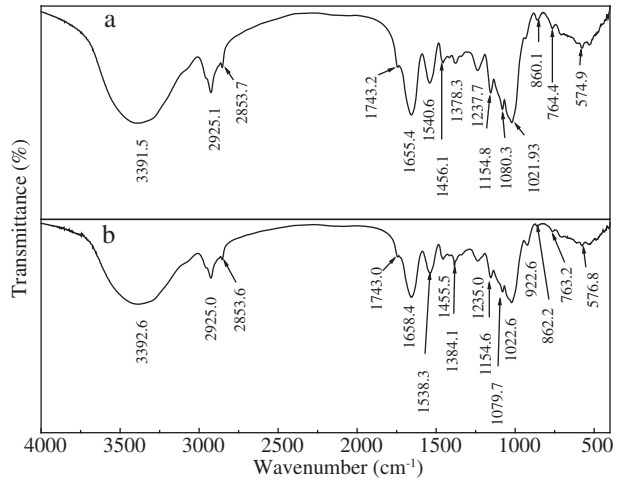

Fig. 4 – FT-IR (Fourier transform infrared spectroscopy) spectra of *S. sporoverrucosus* dwc-3 cells (a) before and (b) after uranium biosorption.

oxygen ligands weekly bonded with uranium (ν(U–O_{ligand})) (Choudhary and Sar, 2011; Kazy et al., 2009).

In conclusion, the overall IR spectra analysis implied that the carboxyl, amide and phosphate groups of *S. sporoverrucosus* dwc-3 cells played a primary role in the bacteria–uranium interaction.

2.5. XPS analyses

To further evaluate the mechanism for biosorption of uranium by *S. sporoverrucosus* dwc-3, the control and uranium-loaded *S. sporoverrucosus* dwc-3 cells were analyzed by XPS. The XPS survey spectrum consisted of carbon, oxygen, nitrogen, phosphorus and uranium peaks. The elemental composition of these samples under study as obtained from XPS analysis is listed in Table 2. It must be noted that the N 1s, P 2p and U 4f peaks were very weak due to their low concentration. The most intense peaks of U 4f (Fig. 5d) appeared at about 381.9 and 392.8 eV and corresponded to the spin–orbit (L–S) split U 4f7/2 and U 4f5/2 states, respectively (Kushwaha et al., 2012).

The C 1s spectra (Fig. 5b) could be decomposed into four components, which are assigned as follows: carbon bound only to carbon and hydrogen (peak 1, C–C, C–H, at 284.6 eV), carbon making a single bond with oxygen or nitrogen (peak 2, C–O, C–N, at 285.9 eV, attributed to alcohol, amine, or amide), carbon making two single bonds or one double bond with oxygen (peak 3, O–C–O, C═O, at 287.3 eV, attributed to amide, and carboxylate), and carbon making one double bond and one single bond with oxygen (peak 4, O═C–OH, O═C–OR, at 288.8 eV, due to carboxyl or ester functions) (Ahimou et al., 2007; Pereira et al., 2013). However, in the case of the uranium-loaded sample, the relative intensity of peaks 2, 3 and 4 greatly changed and the positions of these three peaks were slightly shifted, demonstrating that the uranium mainly interacted with functional groups like amide and carboxylate.

The O1s peaks indicated three different chemical states of oxygen (Fig. 5c) for both the original cells and uranium-loaded cells. The three peaks of the original cells appeared at 531.3, 532.3 and 533.1 eV, which could be attributed to carbonyl oxygen in amide and carboxyl, oxygen atoms in hydroxyls or ethers and oxygen atoms in esters, respectively, which was consistent with the carbon groups (Ahimou et al., 2007; Leone et al., 2006). However, the relative intensity of peak 2 decreased and an increase in the relative intensity in peak 3 was observed in the O 1s XPS spectra of uranium-loaded cells.

Table 2 – Elemental composition determined by X-ray photoelectron spectroscopy.

	Control	Uranium-loaded sample
C	76.72	73.93
O	20.70	23.28
N	1.72	2.13
P	0.86	0.53
U	N.A.	0.13

N.A.: not available since the elemental content is below the minimum detectable limit of the instrument.

Meanwhile, a minor shift of the peaks at 531.3 and 532.3 eV to 531.4 and 533.4 eV indicated the role of amide or carboxyl groups in metal binding.

2.6. SEM-EDS and TEM-EDX analyses

In order to understand the mechanism of complex metal-microorganism interactions, the location of uranium on/in *S. sporoverrucosus* dwc-3 was determined *via* SEM and TEM, combined with energy dispersive X-ray spectroscopy. As shown in Fig. 6, granular aggregate deposits can be clearly observed on the SEM images of the U-adsorbed samples as compared with the control samples. The SEM micrographs also revealed that U-loaded *S. sporoverrucosus* dwc-3 cells changed their cellular morphology. Furthermore, EDS spectra (Fig. 6c) originating from those precipitates exhibited the characteristic peak of uranium, which proved the accumulation of uranium on the external surface of *S. sporoverrucosus* dwc-3. In addition, carbon, oxygen and phosphorus were also observed, as revealed by the EDS spectra.

TEM was employed to verify the distribution and intracellular localization of uranium deposits in *S. sporoverrucosus* dwc-3 cells (Fig. 7). It could be seen that the uranium-free *S. sporoverrucosus* dwc-3 cells showed relatively complete boundaries and homogenous cytoplasm, and no electron-dense granules (Fig. 7a). However, compared to the original *S. sporoverrucosus* dwc-3 cells, *S. sporoverrucosus* dwc-3 exposed to uranium for 12 hr at pH 3.0 displayed the presence of dark electron-dense acicular shapes in the cell interior (Fig. 7b). *S. sporoverrucosus* dwc-3 cells were also analyzed by energy dispersive X-ray (EDX) coupled to TEM, allowing the verification of uranium presence in the dense deposits. The EDX spectra derived from these deposits indicated that they consisted of carbon, oxygen, phosphorus, and uranium (Fig. 7c). The copper peak is from the grid used to support the sections. The lead peak originated from the $Pb(CH_3COO)_2$ used the cell pellet staining. Therefore, the presence of specific peaks for uranium in the uranium-loaded sample confirmed the presence of the absorbed radionuclide.

The distribution of uranium in both cell wall and cytoplasm of the *S. sporoverrucosus* dwc-3 suggested that uranyl ions initially adsorbed on the cell wall and then accumulated in the cytoplasm. Moreover, *S. sporoverrucosus* dwc-3 was identified as a Gram-positive isolate using Gram's staining, which demonstrated that the cell surface consists of abundant carboxyl, amide and especially phosphate functional groups (primarily on the wall teichoic acids and lipoteichoic acids of Gram-positive cell wall). The EDS spectra measured during SEM and TEM indicated the presence of precipitates consisting of carbon and phosphorus, further confirming the interaction of uranyl ions with carboxyl and phosphate groups. The results are consistent with our FT-IR and XPS results. The size of the needlelike granules typically ranged from 50 to 100 nm in length. Our finding was in accordance with other reports (Choudhary and Sar, 2011; Merroun et al., 2006), which also suggested that the intracellular granules in the microorganisms correspond to the polyphosphate bodies studied by TEM. Since electron-dense granules were formed on the cell wall as well as within the cytoplasm of the *S. sporoverrucosus* dwc-3, the process involving the binding

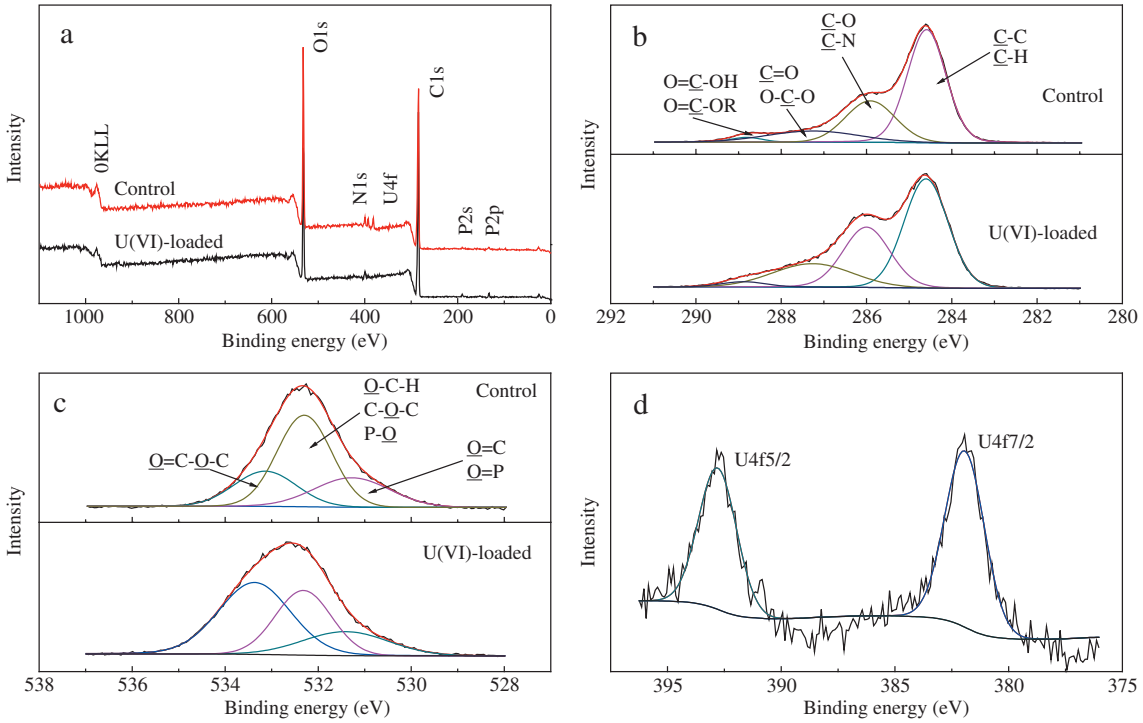

Fig. 5 – X-ray photoelectron binding energy curves of *S. sporoverrucosus* dwc-3. (a) Total survey scans, (b) C 1 s spectra, (c) O 1 s spectra, and (d) U 4f spectra.

of uranyl ions on the surface of the cells could occur by electrostatic interaction with the negatively charged functional groups, for which uranium has a very strong affinity. The uranium was subsequently transported into the cytoplasm through different layers (peptidoglycan, teichoic acids) of the cell wall and cytoplasmic membrane, and gradually formed complexes.

2.7. PIXE and EPBS analyses

Considering that PIXE cannot determine the light elements (atomic number Z < 12), we combined EPBS and PIXE analyses to better understand the full-range elemental composition. The PIXE and EPBS spectra of control cells and uranium-adsorbed cells are shown in Fig. 8. It can be observed that new peaks appear for uranium in the PIXE spectra of uranium loaded samples, but no peaks are observed for Mg, K and Ca. Meanwhile, the distinct peak for uranium was also observed in the EPBS spectra of the uranium-loaded sample (Fig. 8b). The elemental components of *S. sporoverrucosus* dwc-3 and the uranium-adsorbed *S. sporoverrucosus* dwc-3 were calculated from the EPBS and PIXE spectra. As listed in Table 3, the uranium mass percentage was 0.1234 and the content was 0.0036, calculated from the PIXE and EPBS spectra, respectively.

After uranium biosorption, the reduction of the amounts of Mg^{2+}, K^{+} and Ca^{2+} calculated by PIXE might occur because uranium replaced these metal ions in uranium-loaded cells *via* ion exchange. Accompanying metal biosorption, ion (Mg^{2+}, K^{+} or Ca^{2+}) release from the cells was frequently observed,

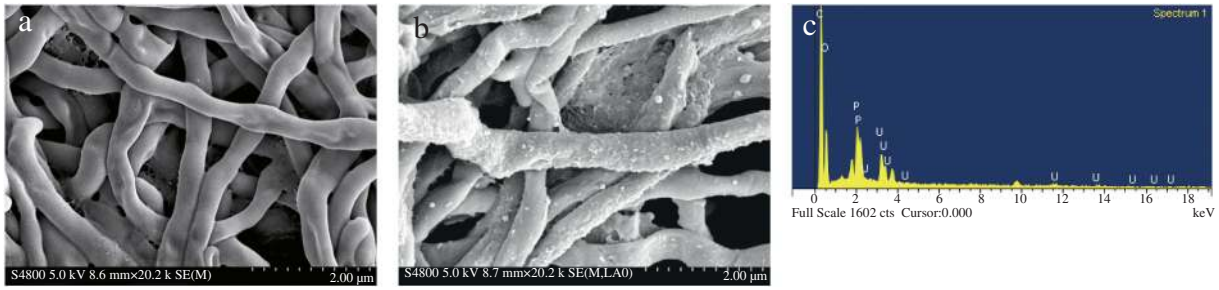

Fig. 6 – SEM (scanning electron microscopy) images of (a) *S. sporoverrucosus* dwc-3 control cells, (b) U-loaded cells and (c) corresponding typical EDS (energy dispersive spectrometer) spectra of U-loaded cells.

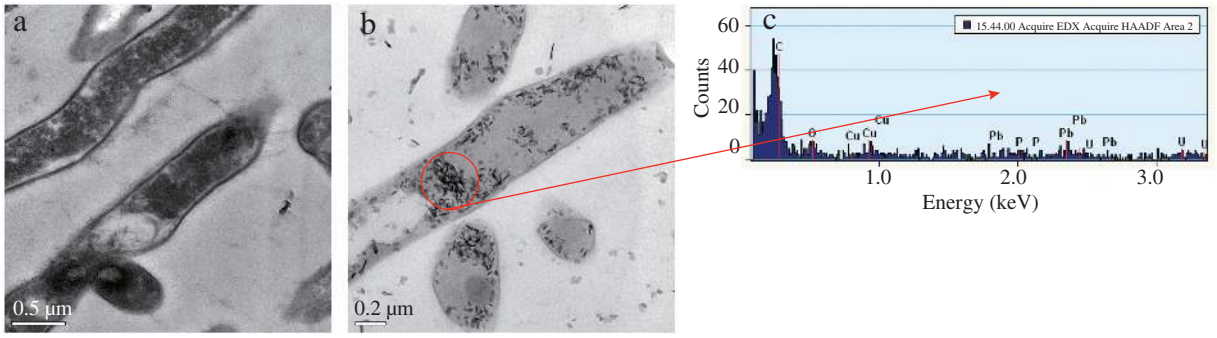

Fig. 7 – TEM (transmission electron microscopy) images of (a) *S. sporoverrucosus* dwc-3 control cells, (b) U-loaded cells and (c) corresponding EDX (energy dispersive X-ray analysis) spectra of deposits.

which suggested that ion exchange could be a relevant mechanism for the binding of metal ions onto the cells. Since the overall charge of the cell must be neutral, any binding of one cation must be accompanied by either stoichiometric release of other cations or by the binding of anions. Several previous reports have demonstrated extensive K release from cells following metal uptake, suggesting K release to maintain ionic balance across the membrane (Choudhary and Sar, 2011; Kazy et al., 2009). Therefore, the above analyses indicated the possibility of uranium binding with the bacteria by displacing cellular potassium through an ion-exchange mechanism.

3. Conclusions

In the present work, we have investigated the uranium biosorption and the mechanisms involved between uranium

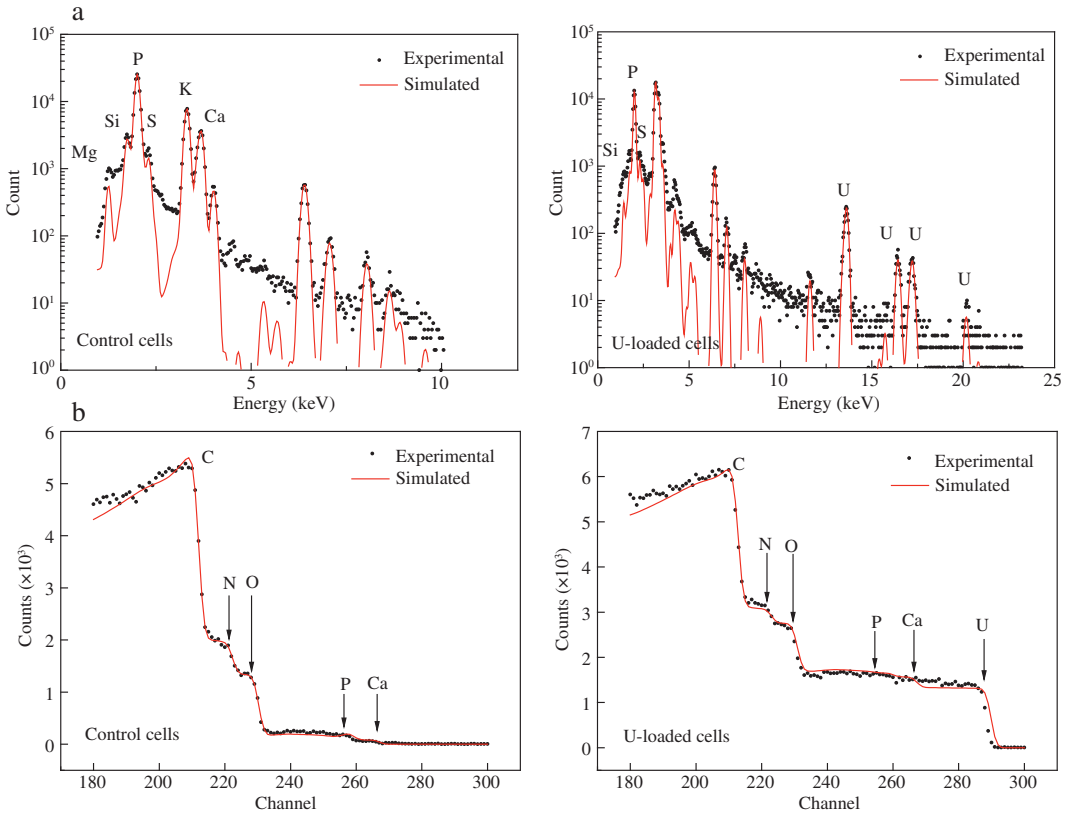

Fig. 8 – (a) PIXE (proton induced X-ray emission) and (b) EPBS (enhanced proton backscattering spectrometry) spectra of *S. sporoverrucosus* dwc-3 control cells and U-loaded cells.

Table 3 – Elemental component of original *S. sporoverrucosus* dwc-3 and U-loaded *S. sporoverrucosus* dwc-3 by proton induced X-ray emission (PIXE) and enhanced proton backscattering spectrometry (EPBS).

Elements	Before biosorption	After biosorption
PIXE results		
Mg	0.0102	N.A.
Si	0.0043	0.0014
P	0.0318	0.0219
S	0.0015	0.0017
K	0.0079	N.A.
Ca	0.0038	N.A.
U	N.A.	0.1234
EPBS results		
C	0.3425	0.3519
N	0.0917	0.0916
O	0.0546	0.0310
P	0.0076	0.0160
Ca	0.0037	0.0118
U	N.A.	0.0036

N.A.: not available since the elemental content is below the minimum detectable limit of the instrument.

and *S. sporoverrucosus* dwc-3, isolated from a potential disposal site of (ultra-)low uraniferous radioactive waste in Southwest China. We found that 12 hr was sufficient to reach sorption equilibrium, and the uranium adsorption capacity was more than 3.0 mg/g *S. sporoverrucosus* dwc-3 (wet weight). The pseudo-second-order kinetic model was applicable to describe the biosorption kinetics. We found that uranium was accumulated as needlelike granules on the cell wall and within the cytoplasm. The possible functional groups of *S. sporoverrucosus* dwc-3 for uranium binding were phosphate, carboxyl and amide groups. PIXE combined with EPBS analyses indicated that ion-exchange was a potential mechanism involved in uranium biosorption by *S. sporoverrucosus* dwc-3.

Acknowledgments

This work was financially supported by the China National Natural Science Foundation (Nos. 21071102, 91126013), Joint Funds of China National Natural Science Foundation and China Academy of Engineering Physics (NSAF, No. U1330125), the State 863 project of China (No. 2012AA063503) and the National Fund of China for Fostering Talents in Basic Science (No. J1210004).

REFERENCES

Ahimou, F., Boonaert, C.J., Adriaensen, Y., Jacques, P., Thonart, P., Paquot, M., et al., 2007. XPS analysis of chemical functions at the surface of *Bacillus subtilis*. J. Colloid Interface Sci. 309 (1), 49–55.

Bai, J., Yao, H.J., Fan, F.L., Lin, M.S., Zhang, L.N., Ding, H.J., et al., 2010. Biosorption of uranium by chemically modified *Rhodotorula glutinis*. J. Environ. Radioact. 101 (11), 969–973.

Chergui, A., Bakhti, M., Chahboub, A., Haddoum, S., Selatnia, A., Junter, G.A., 2007. Simultaneous biosorption of Cu^{2+}, Zn^{2+} and Cr^{6+} from aqueous solution by *Streptomyces rimosus* biomass. Desalination 206 (1-3), 179–184.

Choudhary, S., Sar, P., 2011. Uranium biomineralization by a metal resistant *Pseudomonas aeruginosa* strain isolated from contaminated mine waste. J. Hazard. Mater. 186 (1), 336–343.

Ding, C.C., Feng, S., Cheng, W.C., Zhang, J., Li, X.H., Liao, J.L., et al., 2014a. Biosorption behavior and mechanism of thorium on *Streptomyces sporoverrucosus* dwc-3. J. Radioanal. Nucl. Chem. 301 (1), 237–245.

Ding, C.C., Feng, S., Li, X.L., Liao, J.L., Yang, Y.Y., An, Z., 2014b. Mechanism of thorium biosorption by the cells of the soil fungal isolate *Geotrichum* sp. dwc-1. Radiochim. Acta 102 (1-2), 175–184.

Donat, R., 2009. The removal of uranium (VI) from aqueous solutions onto natural sepiolite. J. Chem. Thermodyn. 41 (7), 829–835.

Freundlich, H.M.F., 1906. Über die adsorption in lösungen. Z. Phys. Chem. 57A, 385–470.

Friis, N., Myers, K.P., 1986. Biosorption of uranium and lead by *Streptomyces longwoodensis*. Biotechnol. Bioeng. 28 (1), 21–28.

Gadd, G.M., Fomina, M., 2011. Uranium and fungi. Geomicrobiol J. 28 (5-6), 471–482.

Golab, Z., Orlowska, B., Smith, R.W., 1991. Biosorption of lead and uranium by *Streptomyces* sp. Water Air Soil Pollut. 60 (1-2), 99–106.

Gorman-Lewis, D., Elias, P.E., Fein, J.B., 2005. Adsorption of aqueous uranyl complexes onto *Bacillus subtilis* cells. Environ. Sci. Technol. 39 (13), 4906–4912.

Han, R.P., Zou, W.H., Wang, Y., Zhu, L., 2007. Removal of uranium(VI) from aqueous solutions by manganese oxide coated zeolite: discussion of adsorption isotherms and pH effect. J. Environ. Radioact. 93 (3), 127–143.

Ho, Y.S., 2006. Review of second-order models for adsorption systems. J. Hazard. Mater. 136 (3), 681–689.

Kaduková, J., Virčíková, E., 2005. Comparison of differences between copper bioaccumulation and biosorption. Environ. Int. 31 (2), 227–232.

Kazy, S.K., D'Souza, S.F., Sar, P., 2009. Uranium and thorium sequestration by a *Pseudomonas* sp.: mechanism and chemical characterization. J. Hazard. Mater. 163 (1), 65–72.

Kushwaha, S., Sreedhar, B., Padmaja, P., 2012. XPS, EXAFS, and FTIR as tools to probe the unexpected adsorption-coupled reduction of U(VI) to U(V) and U(IV) on *Borassus flabellifer*-based adsorbents. Langmuir 28 (46), 16038–16048.

Langmuir, I., 1918. The adsorption of gases on plane surfaces of glass, mica and platinum. J. Am. Chem. Soc. 40 (9), 1361–1403.

Largergren, S., 1898. Zurtheorie der sogenannten adsorption gelosterstoffe. Kungl. Sven. Vetenskapsakademiens. Handl. 24, 1–39.

Leone, L., Loring, J., Sjöberg, S., Persson, P., Shchukarev, A., 2006. Surface characterization of the Gram-positive bacteria *Bacillus subtilis*—an XPS study. Surf. Interface Anal. 38 (4), 202–205.

Li, H.F., Lin, Y.B., Guan, W.M., Chang, J.L., Xu, L., Guo, J.K., et al., 2010. Biosorption of Zn(II) by live and dead cells of *Streptomyces ciscaucasicus* strain CCNWHX 72-14. J. Hazard. Mater. 179 (1-3), 151–159.

Li, L., Hu, Q., Zeng, J.H., Qi, H.Y., Zhuang, G.Q., 2011. Resistance and biosorption mechanism of silver ions by *Bacillus cereus* biomass. J. Environ. Sci. 23 (1), 108–111.

Li, X.L., Ding, C.C., Liao, J.L., Lan, T., Li, F.Z., Zhang, D., et al., 2014. Biosorption of uranium on *Bacillus* sp. dwc-2: preliminary investigation on mechanism. J. Environ. Radioact. 135, 6–12.

Lin, Y.B., Wang, X.Y., Wang, B.P., Mohamad, O., Wei, G.H., 2012. Bioaccumulation characterization of zinc and cadmium by *Streptomyces zinciresistens*, a novel actinomycete. Ecotoxicol. Environ. Saf. 77, 7–17.

Lu, X., Zhou, X.J., Wang, T.S., 2013. Mechanism of uranium(VI) uptake by *Saccharomyces cerevisiae* under environmentally relevant conditions: batch, HRTEM, and FTIR studies. J. Hazard. Mater. 262, 297–303.

Mao, Y.L., Hu, H.W., Yan, Y.S., 2011. Biosorption of cesium(I) from aqueous solution by a novel exopolymers secreted from *Pseudomonas fluorescens* C-2: equilibrium and kinetic studies. J. Environ. Sci. 23 (7), 1104–1112.

Merroun, M., Nedelkova, M., Rossberg, A., Hennig, C., Selenska-Pobell, S., 2006. Interaction mechanisms of bacterial strains isolated from extreme habitats with uranium. Radiochim. Acta 94 (9-11), 723–729.

Mohamed, L.M., Sonja, S.P., 2008. Bacterial interactions with uranium: an environmental perspective. J. Contam. Hydrol. 102 (3-4), 285–295.

Ohnuki, T., Ozaki, T., Yoshida, T., Sakamoto, F., Kozai, N., Wakai, E., et al., 2005. Mechanisms of uranium mineralization by the yeast *Saccharomyces cerevisiae*. Geochim. Cosmochim. Acta 69 (22), 5307–5316.

Ojeda, J.J., Romero-González, M.E., Bachmann, R.T., Edyvean, R.G., Banwart, S.A., 2008. Characterization of the cell surface and cell wall chemistry of drinking water bacteria by combining XPS, FTIR spectroscopy, modeling, and potentiometric titrations. Langmuir 24 (8), 4032–4040.

Pagnanelli, F., PetrangeliPapini, M., Toro, L., Trifoni, M., Veglio, F., 2000. Biosorption of metal ions on *Arthrobacter* sp.: biomass characterization and biosorption modeling. Environ. Sci. Technol. 34 (13), 2773–2778.

Pang, C., Liu, Y.H., Cao, X.H., Li, M., Huang, G.L., Hua, R., et al., 2011. Biosorption of uranium(VI) from aqueous solution by dead fungal biomass of *Penicilliumcitrinum*. Chem. Eng. J. 170 (1), 1–6.

Pereira, P.H.F., Voorwald, H.J.C., Cioffi, M.O.H., Da Silva, M.L.C.P., Rego, A.M.B., Ferraria, A.M., et al., 2013. Sugarcane bagasse cellulose fibres and their hydrous niobium phosphate composites: synthesis and characterization by XPS, XRD and SEM. Cellulose 21 (1), 641–652.

Rho, J.Y., Kim, J.H., 2002. Heavy metal biosorption and its significance to metal tolerance of Streptomycetes. J. Microbiol. 40 (1), 51–54.

Schmeide, K., Sachs, S., Bubner, M., Reich, T., Heise, K.H., Bernhard, G., 2003. Interaction of uranium(VI) with various modified and unmodified natural and synthetic humic substances studied by EXAFS and FTIR spectroscopy. Inorg. Chim. Acta 351, 133–140.

Schmidt, A., Haferburg, G., Schmidt, A., Lischke, U., Merten, D., Ghergel, F., et al., 2009. Heavy metal resistance to the extreme: *Streptomyces* strains from a former uranium mining area. Chem. Erde-Geochem. 69 (S2), 35–44.

Selenska-Pobell, S., Kampf, G., Flemming, K., Radeva, G., Satchanska, G., 2001. Bacterial diversity in soil samples from two uranium waste piles as determined by rep-APD, RISA and 16S rDNA retrieval. Antonie Van Leeuwenhoek 79 (2), 149–161.

Shin, D.C., Kim, Y.S., Moon, J.Y., Park, H.S., Kim, J.Y., Park, S.K., 2002. International trends in risk management of groundwater radio nuclides. J. Environ. Toxicol. 17 (4), 273–284.

Stumm, W., 1992. Chemistry of the Solid–Water Interface: Processes at the Mineral–Water and Particle–Water Interface in Natural Systems. John Wiley & Son Inc., New York.

Suzuki, Y., Banfield, J.F., 2004. Resistance to, and accumulation of, uranium by bacteria from a uranium-contaminated site. Geomicrobiol J. 21 (2), 113–121.

Vijayaraghavan, K., Yun, Y.S., 2008. Bacterial biosorbents and biosorption. Biotechnol. Adv. 26 (3), 266–291.

Vogel, M., Günther, A., Rossberg, A., Li, B., Bernhard, G., Raff, J., 2010. Biosorption of U(VI) by the green algae *Chlorella vulgaris* in dependence of pH value and cell activity. Sci. Total Environ. 409 (2), 384–395.

Wang, J.L., Chen, C., 2006. Biosorption of heavy metals by *Saccharomyces cerevisiae*: a review. Biotechnol. Adv. 24 (5), 427–451.

Wang, J.L., Chen, C., 2009. Biosorbents for heavy metals removal and their future. Biotechnol. Adv. 27 (2), 195–226.

Wang, J.S., Hu, X.J., Liu, Y.G., Xie, S.B., Bao, Z.L., 2010. Biosorption of uranium (VI) by immobilized *Aspergillus fumigatus* beads. J. Environ. Radioact. 101 (6), 504–508.

Williams, K.H., Bargar, J.R., Lloyd, J.R., Lovley, D.R., 2013. Bioremediation of uranium-contaminated groundwater: a systems approach to subsurface biogeochemistry. Curr. Opin. Biotechnol. 24 (3), 489–497.

Xie, S.B., Zhang, C., Zhou, X.H., Yang, J., Zhang, X.J., Wang, J.S., 2009. Removal of uranium (VI) from aqueous solution by adsorption of hematite. J. Environ. Radioact. 100 (2), 162–166.

Yuan, H.P., Zhang, J.H., Lu, Z.M., Min, H., Wu, C., 2009. Studies on biosorption equilibrium and kinetics of Cd^{2+} by *Streptomyces* sp. K33 and HL-12. J. Hazard. Mater. 164 (2-3), 423–431.

Zhang, X., Zhu, Y.G., Zhang, Y.B., Liu, Y.X., Liu, S.C., Guo, J.W., et al., 2014. Growth and metal uptake of energy sugarcane (*Saccharum* spp.) in different metal mine tailings with soil amendments. J. Environ. Sci. 26 (5), 1080–1089.